Article

Ancient Roman Coins from the Republican Age to the Imperial Age: A Multi-Analytical Approach

Caterina De Vito [1,2,*], **Martina Bernabale** [1], **Carlo Aurisicchio** [3], **Fiorenzo Catalli** [4], **Laura Medeghini** [1,2], **Silvano Mignardi** [1,2], **Aida Maria Conte** [2] **and Tilde de Caro** [5]

[1] Department of Earth Sciences, Sapienza University of Rome, P.le Aldo Moro 5, 00185 Rome, Italy; martina.bernabale@uniroma1.it (M.B.); laura.medeghini@uniroma1.it (L.M.); silvano.mignardi@uniroma1.it (S.M.)
[2] Institute of Environmental Geology and Geoengineering, National Research Council (IGAG-CNR), Secondary Office of Rome, c/o Department of Earth Sciences, Sapienza University of Rome, P.le Aldo Moro 5, 00185 Rome, Italy; aidamaria.conte@cnr.it
[3] Institute of Geosciences and Earth Resources (IGG), National Research Council, Secondary Office of Rome, P.le Aldo Moro 5, 00185 Rome, Italy; carlo.aurisicchio40@gmail.com
[4] Via Attilio Friggeri 95, 00136 Rome, Italy; fcatalli@libero.it
[5] Institute for the Study of Nanostructured Materials, National Research Council (ISMN-CNR), Provincial Road 35 d, No. 9-00010 Montelibretti, 00010 Rome, Italy; tilde.decaro@ismn.cnr.it
* Correspondence: caterina.devito@uniroma1.it

Abstract: We report here the results of a multi-analytical approach to characterize twelve Roman coins dating from the third century B.C. to fifth century A.D. that were found in the surroundings of Rome and for which the year of minting is determined by numismatic analysis. The coins were studied using SEM-EDS, EMPA, XRD, and FTIR techniques, enabling semi-quantitative and quantitative determinations of the chemical and mineralogical composition of the alloys and corrosion products. SEM-EDS analyses highlighted the occurrence of corrosion products on the surfaces and wide chemical variations due to selective enrichment or depletions of the alloying metals. The EMP analyses showed that three of the twelve coins are made of copper (1), one is a copper–tin alloy (2), five are copper–tin–lead alloys with elements in different proportions (3), two are copper–lead alloys (4), and another one is a *subaerata* coin (5). In addition, the physical parameters of the coins, i.e., density, weight, and diameters, were measured to have an overall characterization.

1. Introduction

Ancient Roman bronze coins attracted the attention of numerous specialists in the field because of their important role in studies focused on history or on aspects of manufacturing as well as on the compositional and metallurgical features and corrosive patterns [1,2]. Furthermore, detailed analytical studies of the coins provide an accurate understanding of the Romans' knowledge of the chemical and physical properties of metals [3–5].

The Romans needed to conquer new territories to supply the sources for metal artifact production and control their resources. An interesting example of this is the occupation of Britain; historians report that this region's occupation was necessary for controlling tin deposits in the ancient world. Indeed, tin was essential to producing bronze, which was extensively used for both commercial exchange and decorative items [6,7].

A numismatic analysis is also essential to date historical events, reconstruct trade routes, and evaluate the welfare of the Roman society's economy and social life over the centuries [8–15]. This work aims to investigate the chemical composition of twelve selected coins used in daily transactions and wide diffusion that were found in archaeological sites near Rome. These coins cover a time frame going from the third century B.C. to the fifth century A.D.

2. Coinage Background

At the beginning of the fourth century B.C., Rome had a primitive bronze coinage because the early Roman bronze "coins" consisted of bars and discs for daily commercial transactions. Coinage in the Early Roman Period, as referred to by [10], appeared at the end of the fourth century B.C. Crawford (1974) proposed [8] that this event took place halfway through the third century B.C. Historians suggest that in this period an important transition took place in commercial practices and trade exchanges, i.e., payment with metal bars gave way to coins. The new payment system based on coins developed rapidly, with the issue of many different types. Over the centuries, coins underwent several changes in shape, value, and weight according to the evolution of the Roman economy [12].

Rome operated several monetary systems during its long history, i.e., the early Republican monetary system before the Second Punic War (219 B.C), the Republican monetary system from the Second Punic War until the end of the Republic (27 B.C), and the Imperial monetary system [8]. During the Roman Republic, coinage was largely influenced by Greek culture, particularly the mints of the "Romano-Campano" area, which belonged to the Magna Graecia before the Roman expansion [13,14].

Later, the Imperial monetary system permitted the minting of official false *subaerata* coins, which were produced in mints away from Rome by the authorities during the crisis [15].

The most commonly minted coins in Rome and its provinces were made of copper or bronze, a copper and tin alloy in various proportions, and generally containing minor amounts of other metals such as Pb, Fe, As, and Ag. Because of their small value and widespread diffusion, one can expect that the components of bronze were brought to Rome. For this reason, coins are the best indicators for tracing the ore sources and the patterns of trading to acquire metals used by the Romans. On the other hand, gold and silver coins had very limited distribution, with some exceptions related to the incorporation or occupancy of new regions having ready sources of precious metals, or to the celebration of an important historical event [8].

During the Roman Republic and Empire, mining operations existed from Spain to Cyprus and from Britain to Sardinia [7]. These mines provided gold, silver, copper, zinc, lead, iron and, of course, tin (Figure 1). The metals were used to equip the army, mint coins, build cities, and make everyday items. The mining, refining, and use of metals were at the core of the Roman Empire.
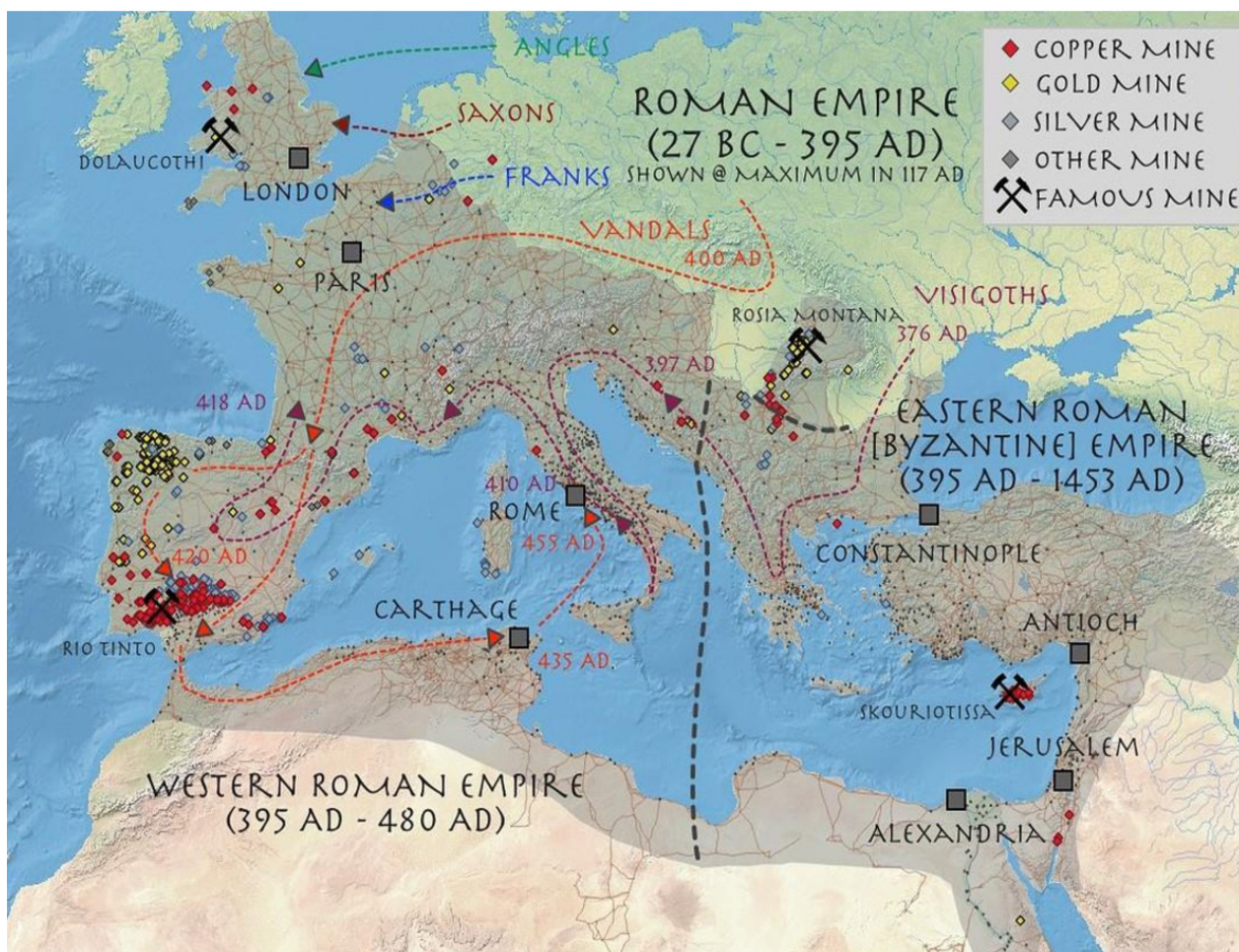
Figure 1. Location of the main mines along the Roman Territories during the Roman Empire (from Wilson, A. and Friedman, H. (2010) [16]. Mining Database. Version 1.0. Accessed (26 November 2023): http://oxrep.classics.ox.ac.uk/databases/mines_database/).

The commonly used tool in archaeometry to trace sources of raw materials for metals and alloys is the measurement of lead and copper isotopes [17–21]. Some ambiguity about relating archaeological objects to ore deposits remains in many cases, because of the possibility of mixing ore or metal from various deposits and re-melting of old metal objects. These practices obscure the fingerprints of the supplying orebodies.

The use of major and trace elements to fingerprint and explore the technical advancements in smelting and refining processes was demonstrated by [22–24] for Roman copper coinage and [25] for the Celtic gold coins.

Studies of archaeological objects can also improve knowledge in the field of long-term corrosion, helping scientists and curators to control and arrest the process of deterioration of ancient metal objects and selecting ideal storage conditions in museums [26,27].

A great wide variety of alteration products have been found in copper and bronze artifacts depending on the influence of the environment of conservation, e.g., burial, soil [28,29]. Corrosion of archaeological bronze has been extensively studied to identify the nature of the corrosion products in response to various corrosive media and improve knowledge in the field of long-term corrosion to preserve metallic artifacts from further degradation.

All these studies are useful in different fields, particularly for the restoration and conservation of metal artifacts. Recently, research into green corrosion inhibitors showed interesting results after their application on metal artifacts, revealing a dependence on the chemical composition of the alloy. Indeed, corrosion inhibitors represent one of the new

methodologies used to preserve metallic cultural heritage and are intricately linked to the specific alloy composition [30–32].

Recently, new non-invasive techniques were introduced to explore corrosion mechanisms in archaeological artifacts which are useful for exploring corrosion, plastic, and aplastic deformations of archaeological artifacts [26,27,33].

3. Metal Deposits Available in Ancient Roman Time

The coins investigated here were minted over a long period, ranging from 235 B.C. to 518 A.D., and were grouped based on their chemical composition, e.g., copper, copper–tin alloy, copper–tin–lead alloy, copper-leaded, and one *subaerata* coin.

As these coins were widely diffused in Rome and in its provinces, the control of mineral resources was crucial for the development of the Roman economy. During the Roman Republic, the coins circulating in the Italian Peninsula were mainly made of copper and bronze. As bronze contains essential tin, the tin resources of the Mediterranean world are an important element needed to reconstruct the trade routes of this metal, which was extensively used by the ancient people, starting from the Bronze Age.

The possibility of important sources of tin located in the western Mediterranean has been discussed for a long time and the mysterious "Tin Islands" (Kassiterides) are vaguely documented [34]. Important tin resources occurred in Iberia, especially in northern Portugal, Brittany (France), and German, where they were mined at different times [35,36].

The Romans imported lead, another metal for coinage, from several active mines in the Mediterranean world [19,20]. Ancient bronze coins began to be heavily "leaded" in the third century B.C. [7]. Indeed, the main advantage of lead addition is that the molten bronze becomes more mobile, which allows for a better hollow casting.

Under the Roman Empire, the main metal-producing base metals deposits were in Sardinia, Spain, Great Britain, Cyprus, Illirian Albania, Yugoslavia, and others in Nord Africa [37,38]. During the Augustan-Tiberian age (29 B.C.–37 A.D.), ore minerals came from Sardinia and southern Spain, where mines of copper were active. In the early Augustan period, Sardinia was a major copper producer, but it was later replaced by resources from Spain and Cyprus. In the Tiberian time, the mining activity in Spain involved the Rio Tinto deposit, which had become the main site of copper production by the end of the Tiberian period; moreover, other mines in Spain were exploited for copper, along with the deposits occurring in Sierra Morena. For the first time during the reign of Tiberius, sources of copper were documented from Cyprus [24].

Later, during the Roman Empire, the deposits of Cornwall and Devon were the main tin-producing provinces. Both sites have alluvial deposits of cassiterite, which are relatively easy to mine. Lead mining occurred extensively in Germany [35]. Given the numerous lead artifacts found there, Germany is now considered to have been an important source of lead ore supplying Rome in the period being considered.

4. Materials and Methods
4.1. Materials

Twelve Roman coins, minted in the period ranging from 235 B.C. to 518 A.D., are investigated through a multi-analytical approach.

Optical and scanning electron microscopies were used to acquire numismatic data [8,9] and the surface condition of each coin (e.g., wear, corrosion). These examinations revealed that most of the coins were subject to wear caused by their use and burial conditions (from moderate to severe), and this resulted in some cases in a loss of detail from the coin's design and a loss of the plating layer. However, the designs that remain were sufficient to classify them as *Aes Litra* (#1), *Rostrum tridens Aes* (#2), *Sextans Mercurius*/bow (#3), *Augustus As* (#4), *Claudius As* (#5), *Quadrans of Caligola* (#6), *Sextertius* of Alexander Severus (#7) *Sextertius* of Philippus Caesar the II (#8), *Divus Claudius Goticus* and *Quintillus As* (#9), *Nummus radians* of Galerius Caesar (#10), *Nummus* of Valens (#11), and Anastasius I *Follis* (#12). More details and relative ages are reported in Table 1.

Table 1. Pictures and numismatic characterization of the selected coins.

	Coin's Pictures	Name	Value	Ø mm	Age	Mint	Reference	Inscriptions
1		Aes Litra	As	15.58	241–235 B.C.	Rome	Crawford 25/3; Sydenham 26; BMCRR (Romano–Campanian) 64	O/Helmeted heA.D. of Mars right; R/Horse's heA.D. right, strigel/sickle behind, ROMA below
2		Rostrum tridens Aes	As	32.38	206–195 B.C.	Rome	Crawford 114/2; Sydenham 245	O/Laureate heA.D. of Janus right, I above; R/Prow right, Rostrum Tridens right and I above, Roma below
3		Mercurio/Prua	Sextans	19.33	211–208 B.C.	Rome	Crawford 61/6; BMC Italy 345	O/HeA.D. of Mercurius right; R/
4		Augustus	As	25.62	27 B.C.–14 A.D.	Rome	RIC 435	O/CAESAR AUGUST PONT MAX TRIBUNIC POT bare heA.D. right; R/M MAECILIUS TVLLVS III VIR AAA FF around SC
5		Claudius	AS	27.46	41– 50 A.D.	Rome	RIC I, 97	O/TI CLAUDIUS CAESAR AVG PM TR P IMP testa di Claudio a sx; R/LIBERTAS AVGUSTAS Personificazione della Libertas stante, ai lati SC
6		Caligula	QuA.D.rans	16.47	40–41 A.D.	Rome	RIC 52; BMC 64	O/C CAESAR DIVI AUG PRON AUG, in the middle a pileus between the letters S C; R/PON M TRP IIII PP COS TERT, the middle bears the letters R C C
7		Severus Alexander	Sestertius	25.34	231–235 A.D.	Rome	RIC IV–2, 523; Cohen 421	O/IMP ALEXANDER PIVS AVG, laureate bust right, draped on far shoulder; R/P M TR P X COS III S–C, Victory standing left, holding wreath and palm.
8		Philippus II Caesar	Sestertius	29.65	244–246 A.D.	Rome	RIC 256a; Cohen 49	O/M IVL PHILIPPVS CAES, draped bust right; R/PRINCIPI IVVENT S–C, Philip II standing left with globe & spear
9		Divus Claudius II Gothicus	Antoninianus	17.55	ca 270 A.D.	Milan	RIC 261, Cohen 50	O/DIVO CLAVDIO, rA.D.iate heA.D. right; R/CONSECRATIO, large flaming, garlanded altar
10		Galerius Maximian	RA.D.iate Fraction	20.77	296–297 A.D.	Alexandria	RIC VI 48b	O/GAL VAL MAXIMIANVS NOB CAES, rA.D.iate, draped bust right; R/CONCORDIA MIL–ITVM, Galerius standing right receiving Victory on globe from Jupiter. B in centre
11		Valens	Nummus	17.6	364–378 A.D.	Cyzicus	RIC 11b	O/DN VALEN–S PF AVG, pearl diA.D.emed, draped, cuirassed bust right; R/SECVRITAS–REIPVBLICAE, Victory A.D.vancing left holding wreath and palm. SMK and officina letter A to delta in ex
12		Anastasius I	Follis (40 nummi)	32.33	491–518 A.D.	Constantinople	Morrison 27	O/D N ANASTA–SIVS P P AVG, diA.D.em &draped bust right; R/large M, cross above, star to either side, officina letter Γ below, CON in ex.

4.2. Methods

We used micro and non-destructive techniques, including scanning electron microscopy (SEM-EDS), electron microprobe analyses (EMPA), X-ray diffraction (XRD), Fourier-transform infrared spectroscopy (FTIR), and density determination to characterize the surface morphology, chemical composition, and alteration products. This approach allows for a complete compositional characterization of the surface of the coins by sampling a very small spot (≤ 5 µm). In this way, we have been able to stress, with high accuracy, the extreme heterogeneity of the alloys used for coinage over many centuries by the Romans.

First of all, the coins were gently mechanically cleaned (ultrasonic) to remove the earth and traces of dirt. The coins were preliminarily studied using optical microscopy (OM) in reflected light to acquire information on surface and corrosion. Then, they were investigated via scanning electron microscopy (SEM-EDS) using a ZEISS system operating at 20 kV equipped with X-ray energy-dispersive spectroscopy (EDS). To evaluate the compositional heterogeneity of a sample's surface, back-scattered electron images (BSE) were used.

The analyses of Cu, Sn, Pb, and other metals were acquired at the surfaces using electron probe microanalysis (EMPA). Analyses have been carried out along one of the diameters of each coin (one spot every about 500 µm, where possible). EMPA was performed on micro-areas previously polished with a micro drill. It is a suitable technique for quantitative chemical composition because it has a high resolution (1–2 µm) and low detection limit (ca. 0.02%). The analyses were carried out using a Cameca Cx 827 electron microprobe equipped with three wavelength dispersion spectrometers (WDS) and one energy dispersion spectrometer (EDS, Link Systems AN 10000/85S). All the coins were analyzed with an accelerating voltage of 15 kV, a sample current of 30 nA measured on synthetic andradite, and a beam diameter of 3–5 µm. Wavelength dispersion spectrometers were used for all elements, whereas the energy dispersion system was used only to collect qualitative information on the average composition of each sample. We used $K\alpha$ lines for Cu, Fe, Zn, Co, and Ni, $L\alpha$ lines for Sn, As, Ag, Cd, Sb, and Mo, and $M\alpha$ lines for Pb, Bi, and Au. The intensities of the peaks and backgrounds were each counted for 10 s for major elements and 20 s for minor and trace elements. Pure metals were used as reference standards for each element to obtain quantitative compositions. The analytical data were reduced and corrected using the ZAF-FLS method. The intensities obtained are associated with an analytical error of ~1% relative to major elements and ~5% relative to minor elements. The detection limits under the working conditions specified a range between 0.05 and 0.1 wt.%.

X-ray diffraction (XRD) patterns were obtained on the whole of six coins using a Seifert diffractometer operating at 40 kV and 30 mA. The XRD patterns were recorded from 5° to 60° 2θ at a rate of 0.02° per step and with a counting time of 8 s per step using Cu $K\alpha$ radiation.

IR-scope II (Bruker) collected micro-FTIR transmittance spectra in the range 4000–600 cm^{-1} to characterize the functional groups of the corrosion-induced compounds. The spectra were recorded in the transmittance mode with a resolution of 2 cm^{-1}; we accumulated 200 scans, with a beam diameter of about 20 µm.

The measurements of the density of each coin were carried out using a Westphal hydrostatic balance. Finally, the weight of each coin was measured using an analytical balance with an accuracy of four decimal places.

5. Results

5.1. SEM-EDS

SEM-EDS investigation on selected coins gives information on surface microstructure, chemical compositions, and corrosion patterns. SEM-EDS images of coin #1 (Figure 2) highlighted the occurrence of a Cu-Sn binary alloy (spectrum 1), having As content in a minor amount (spectrum 2). This coin shows areas with Sn enrichments and Cu depletions on the surface (spectra 2 and 3). In addition, the surface presents moderate pitting and metal loss.

The SEM-EDS spectra of coins #2, #7, #9, and #12 revealed the occurrence of complex chemical compositions of the alloys, exhibiting Cu-Sn-Pb-Fe. In particular, coin #7 shows complex patterns of metal enrichments and depletions on the surface (spectra A, B, C)

(Figure 3). Also, the structures of the surfaces of these coins present pitting corrosion and metal loss (Table 1).

The X-ray maps of coins 7 and 12 (Figure 4) highlighted important variations in metal concentrations on the surfaces due to the corrosive process. As shown in Figure 4, SE images (gray color) evidence the loss of materials and corrosion products. In addition, X-ray maps show an inhomogeneous distribution of metals in the investigated areas, where the brilliant or dull colors indicated high or low concentrations of a given metal.
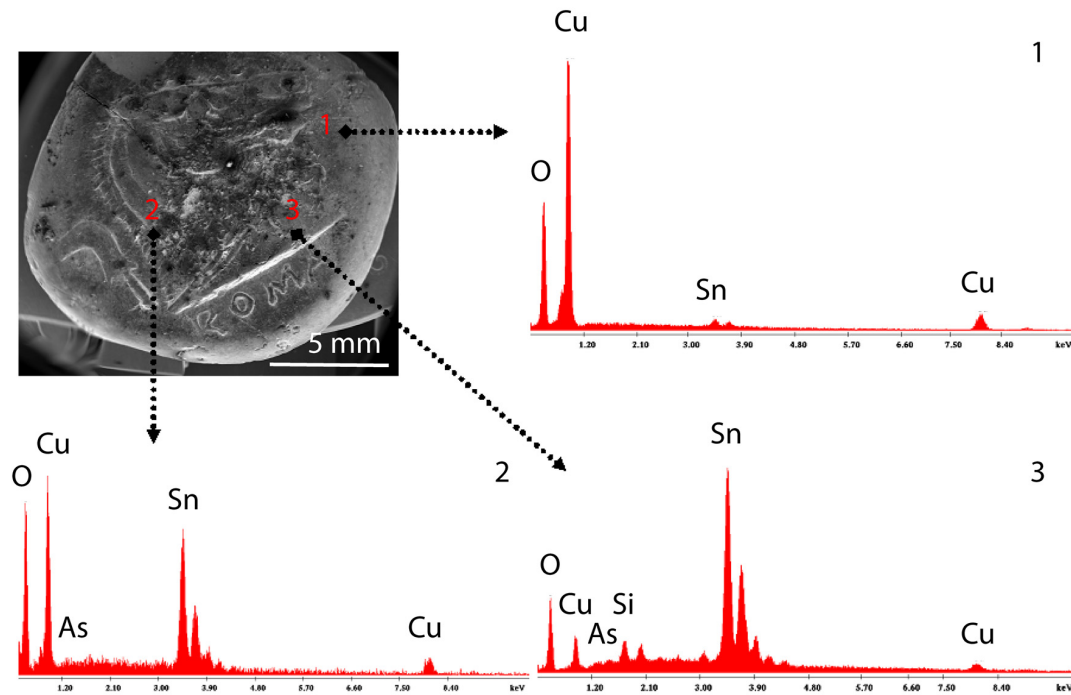

Figure 2. SEM image of coin #1 and EDS spectra: (**1**) Cu-enriched area and (**2**,**3**) Sn-enriched surface.
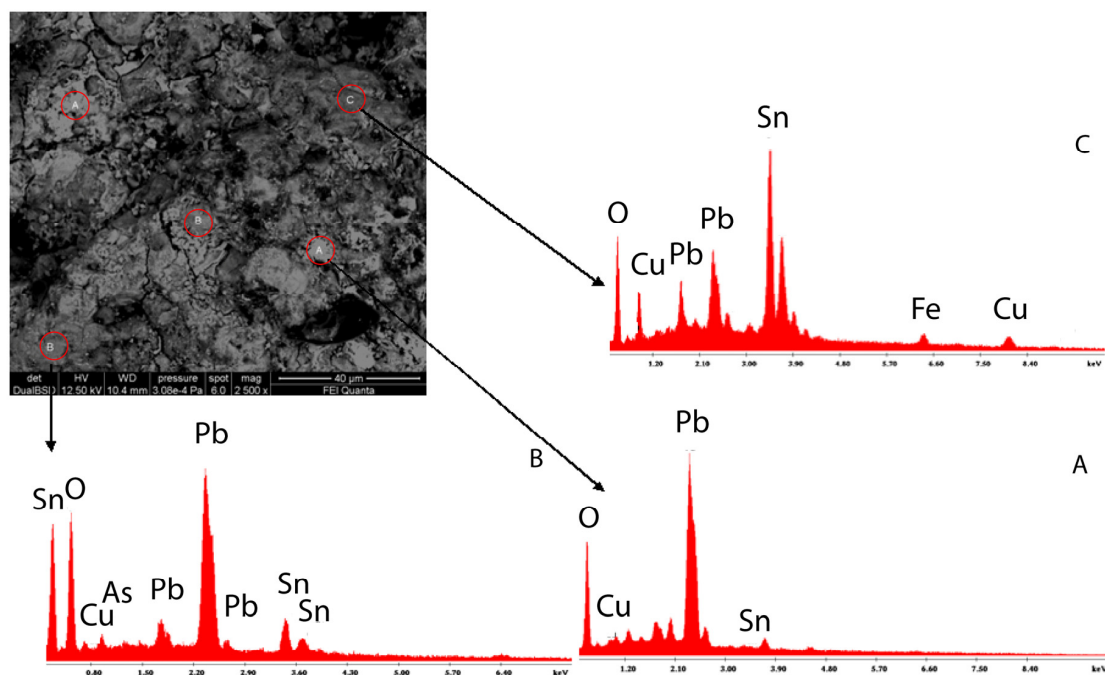

Figure 3. SEM image of coin #7 and representative EDS spectra of different micro-areas on the surface: (**A**) Pb-rich areas (**B**) Pb-Sn-rich areas and (**C**) Sn-Pb-Cu-rich areas.
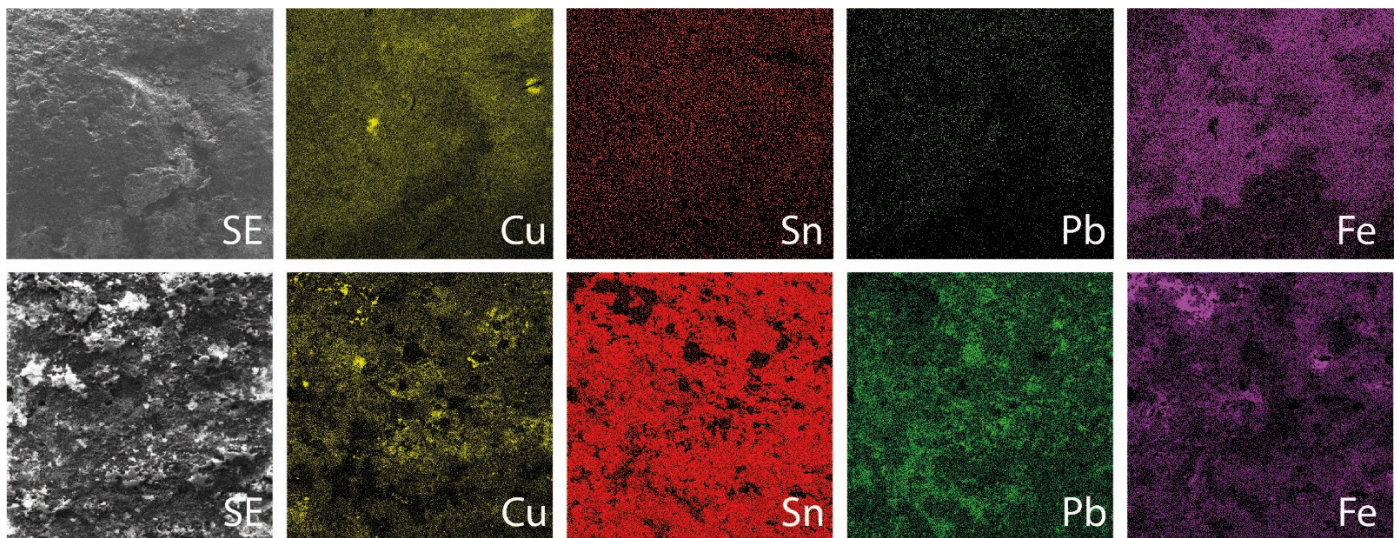
Figure 4. SE images of coins #7 and #12 and X-ray maps of Cu, Sn, Pb, and Fe.

5.2. EMPA

The EMP quantitative chemical analyses acquired on the surfaces (Table 2) and along the well-defined profiles of the coins (Figure 5) permitted five groups to be distinguished: (1) copper, (2) copper–tin alloy, (3) copper–lead alloy, (4) copper–tin–lead alloy, and, finally, group (5) which is represented by one *subaerata* coin composed of a thin copper sheet applied on a lead substrate.

Table 2. Representative chemical compositions (mass %) of the twelve Roman coins.

Coins	Cu	Sn	Pb	Fe	Zn	Ag	As	Cd	Co	Ni	Sb	Au
Group 1												
Augustus (#4)	99.55	bdl	bdl	bdl	bdl	bdl	bdl	bdl	bdl	0.05	bdl	bdl
Caligula (#6)	98.87	bdl	0.37	0.50	0.01	0.03	0.05	bdl	0.03	0.04	bdl	bdl
	99.48	bdl	0.28	0.05	bdl	0.05	0.05	0.01	0.02	0.04	0.02	bdl
Galerius Maximian (#10)	96.53	0.05	0.42	2.20	0.11	0.69	bdl	bdl	bdl	bdl	bdl	bdl
	98.12	bdl	0.78	0.99	bdl	bdl	0.02	bdl	0.07	0.02	bdl	bdl
	97.93	0.28	1.08	0.30	0.02	bdl	bdl	0.03	bdl	bdl	0.36	bdl
Group 2												
Aes Litra (#1)	31.32	67.02	0.17	0.17	bdl	0.02	1.07	bdl	0.09	0.14	bdl	bdl
	44.53	52.03	0.43	2.12	bdl	0.09	0.52	bdl	0.14	0.14	bdl	bdl
	5.40	93.67	0.03	0.41	bdl	bdl	0.20	0.02	0.13	0.15	bdl	bdl
Group 3												
Rostrum tridens Aes (#2)	24.38	40.27	27.88	6.80	bdl	bdl	0.53	0.13	bdl	bdl	bdl	bdl
	6.09	55.08	31.78	6.29	bdl	0.23	0.37	0.16	bdl	bdl	bdl	bdl
	72.34	9.71	10.33	6.94	bdl	bdl	0.36	0.32	bdl	bdl	bdl	bdl
Mercurius/Prora (#3)	68.14	5.89	25.00	0.42	0.06	bdl	0.37	bdl	0.09	0.03	bdl	bdl
	0.38	0.03	99.11	0.35	bdl	bdl	bdl	0.04	0.04	0.04	bdl	bdl
	17.90	47.03	22.31	12.65	0.03	0.03	bdl	bdl	bdl	0.04	bdl	bdl
	96.96	0.06	2.70	0.11	0.03	0.03	0.02	0.03	0.03	0.02	bdl	bdl
Severus Alexander (#7)	86.57	3.13	6.44	3.78	bdl	0.08	0.00	bdl	bdl	bdl	bdl	bdl
	58.38	18.04	16.41	1.92	0.56	0.36	0.26	bdl	0.07	0.34	3.76	bdl
	70.81	5.57	21.78	1.33	bdl	0.10	0.25	0.01	0.02	0.11	bdl	bdl
Philippus II Caesar (#8)	10.61	67.65	18.46	3.08	0.06	0.06	0.02	bdl	0.06	bdl	bdl	bdl
	54.67	28.00	9.23	7.82	0.10	bdl	0.06	bdl	0.08	0.04	bdl	bdl
	12.63	65.36	10.57	11.25	0.11	bdl	bdl	bdl	bdl	bdl	bdl	bdl
Divus Claudius II Gothicus (#9)	80.95	7.26	10.75	0.02	0.41	0.60	bdl	bdl	bdl	bdl	bdl	bdl
	96.41	0.02	0.39	0.14	bdl	3.04	bdl	bdl	bdl	bdl	bdl	bdl
	49.36	7.99	39.67	1.05	bdl	1.92	bdl	bdl	bdl	bdl	bdl	bdl
	93.25	0.26	5.20	0.98	bdl	0.31	bdl	bdl	bdl	bdl	bdl	bdl

Table 2. *Cont.*

| Coins	Cu	Sn	Pb	Fe	Zn	Ag	As	Cd	Co	Ni	Sb	Au
Group 4												
Claudius (#5)	96.08	0.12	2.74	0.25	0.12	0.19	0.19	bdl	bdl	bdl	0.31	bdl
	74.26	bdl	18.73	4.43	bdl	bdl	bdl	bdl	bdl	0.28	0.46	1.48
Anastasius I (#12)	63.74	0.26	6.85	27.94	0.07	0.20	0.42	bdl	bdl	bdl	0.52	bdl
	88.60	bdl	1.51	9.40	bdl	0.26	0.09	bdl	bdl	bdl	0.14	bdl
	94.27	bdl	4.17	0.13	bdl	0.25	1.11	bdl	bdl	bdl	0.07	bdl
	63.76	0.18	3.24	30.45	bdl	0.09	0.18	0.09	bdl	0.57	1.38	bdl
Group 5												
Valens (#11)	98.79	0.27	bdl	0.06	bdl	0.13	0.51	0.00	0.01	0.08	0.15	bdl
	1.34	1.56	96.31	0.38	bdl	0.03	0.10	0.15	bdl	bdl	0.12	bdl
	0.84	0.74	97.99	0.17	bdl	bdl	bdl	0.14	bdl	bdl	0.12	bdl
	99.61	0.11	0.06	0.05	bdl	0.03	0.06	0.05	bdl	0.03	bdl	bdl
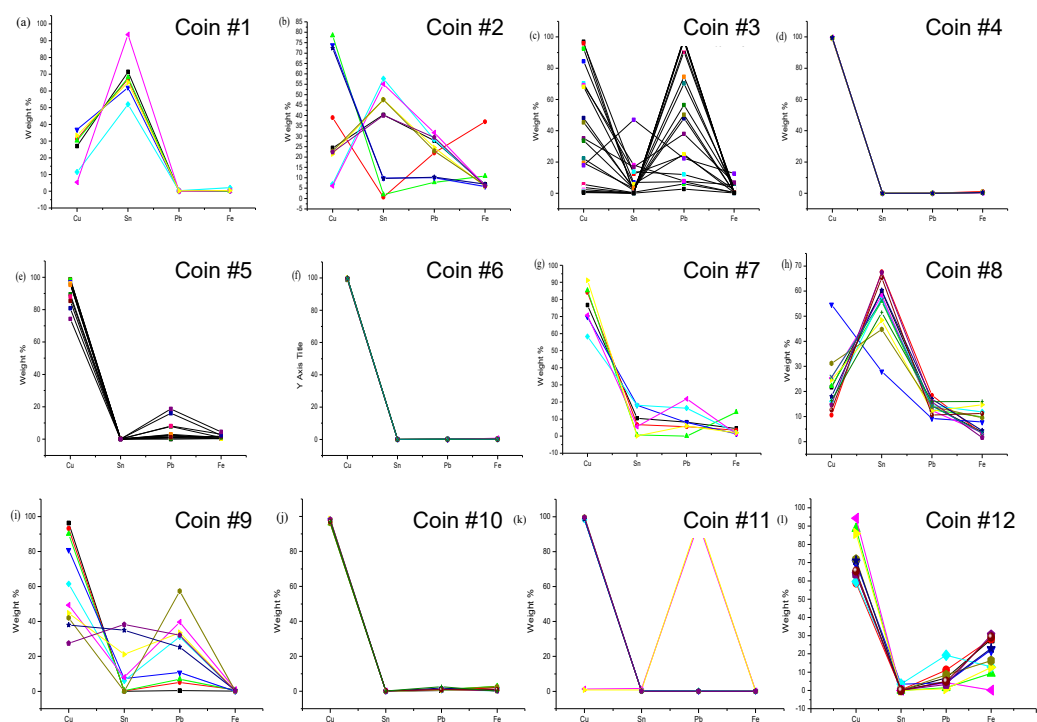
Figure 5. Binary diagrams of the major elements of all coins. (**a**–**l**) The colored lines represent compositional variations of different point analysis along selected profiles.

Group 1 is composed of coins having the highest Cu content, i.e., Augustus As (#4), Quadrans of Caligula (#6), and Nummus radians of Galerius Caesar (#10) (Table 2). The Cu content ranges from 96.5 wt.% to 99 wt.%, with minor amounts of Pb, Sn, Fe, and Zn.

The Aes Litra (#1) of Group 2 is a copper–tin alloy in which Sn is the more abundant element on the surface (52–94 wt.%) followed by Cu (0–35 wt.%) due to two selective enrichments or depletions in corrosive areas. Minor and trace elements such as Pb, Fe, As, Co, and Ni also occur (Table 2).

The Rostrum Tridens Aes (#2), Sextertius of Alexander Severus (#7), Sextertius of Philippus Caesar the II (#8), and Divus Claudius Goticus and Quintillus As (#9) of group 3 consist of a ternary Cu-Sn-Pb alloy displaying a complex distribution of elements (Table 2). In detail, Cu and Pb prevail over Sn in coins #3 and #9, whereas coin #7 shows Cu as the most abundant element. The abundances of Sn and Pb are similar and range from 0 to 20%. In coin #8, Sn predominates over Cu and Pb, whereas in coin #2, the three elements are randomly distributed (Table 2). Moreover, coin #9 of group 3 shows the lowest Fe contents (0.02–1.05 wt.%) and significant amounts of Ag (0.33–3.04 wt.%). Traces of Zn are present in all coins of group 3.

Group 4 comprises three coins, Claudius As (#5), Sextans Mercurius/Prow (#3), and Follis of Anastasio I (#12), and all are Cu-Pb alloys. These coins display Cu enrichment (up to 98%) on the surface, whereas in the inner part, a significant amount of Pb occurs (up to about 20 wt.%); minor amounts of Sn, Ag, As, and Sb also are present (Table 2). Coin #11, Nummus of Valents, is a special case (i.e., a *subaerata* coin, group 5) that displays two distinct compositions: one part made up almost exclusively of copper and the other one of Pb. Minor amounts of Sn and trace amounts of Ag, As, and Sb are also present. Another feature of some coins (#2, #3, #5, #7, #8, #12) is the presence of Fe, which is up to 20 wt.%.

5.3. XRD, FTIR, and Density

The X-ray diffraction patterns of four selected coins were performed on the surfaces (Figure 6), suggesting the presence of different crystalline phases identified as oxides (Cu and Sn), Pb carbonate (cerussite and hydrocerussite), and Cu carbonate hydroxide (malachite) and trace of $CuAl_2O_4$ spinel.
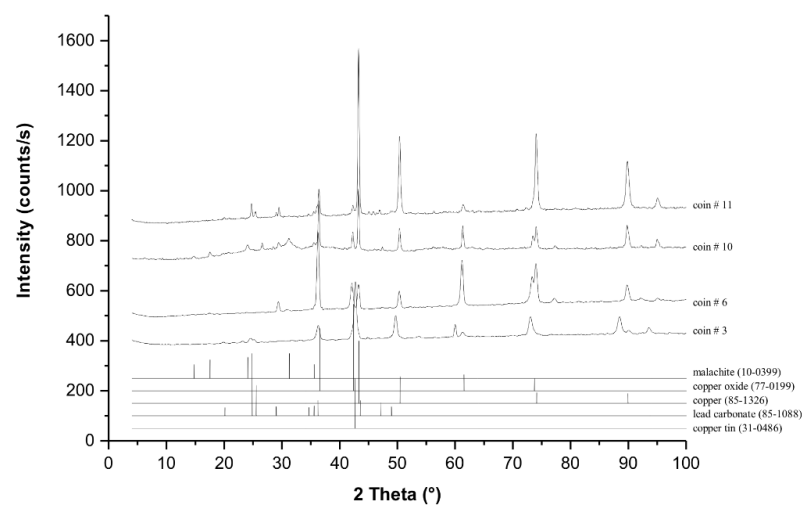
Figure 6. XRD patterns of four coins compared with the strongest lines recorded in JCPDS cards.

FTIR spectra of the green compounds, which cover many coins, indicated a mixture of malachite $[Cu_2(CO_3)(OH)_2]$ and hydrocerussite $[2PbCO_3 \cdot Pb(OH)_2]$ (Figure 7). The identification of these corrosion minerals was made using FTIR literature cards [39].
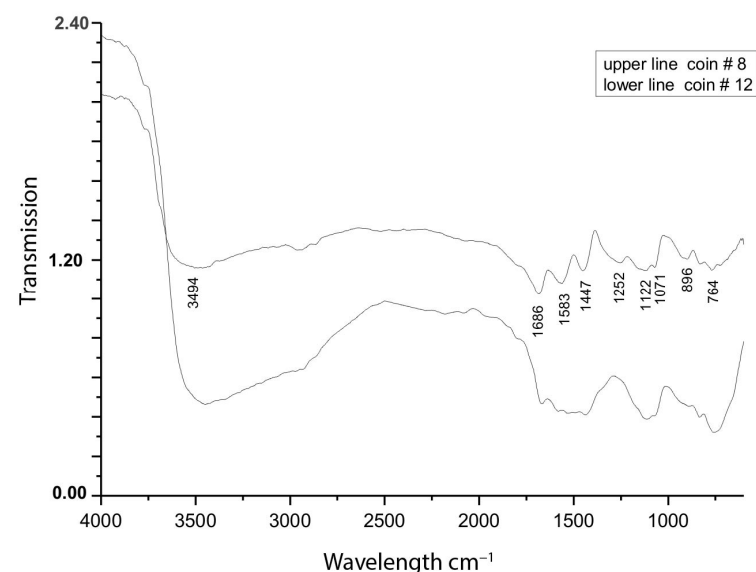
Figure 7. IR spectra of green compounds on coins #8 and #12.

The measured density of the coins of all samples ranges from 7.656 to 8.914 g/cm^3. In contrast, the calculated (theoretical) ones vary from 7.789 to 9.196 g/cm^3 (Table 3, Figure 8). These former densities of all the coins were calculated using EMP compositions and phase abundances indicated by XRD patterns.
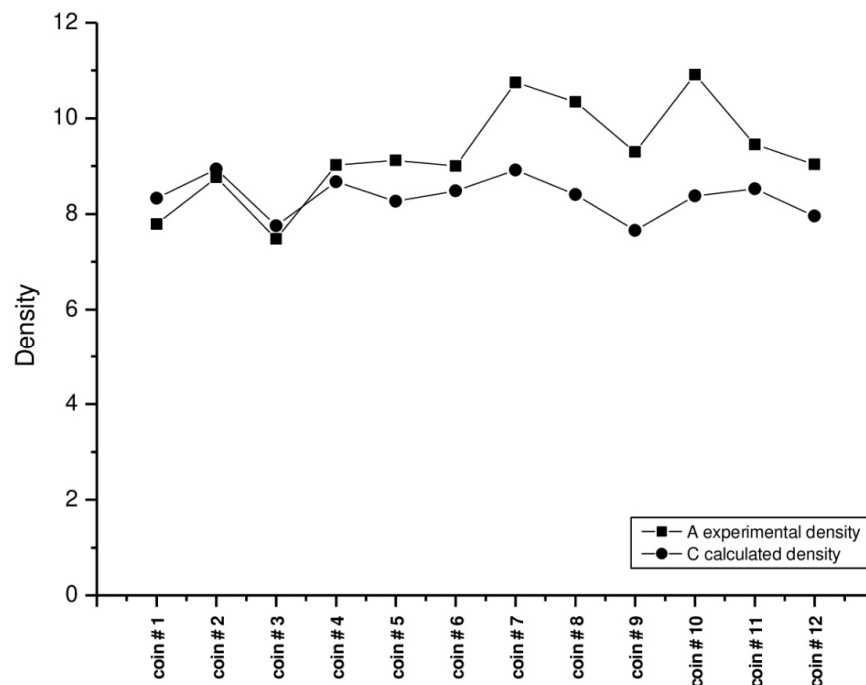

Figure 8. Trends of the experimental and calculated density of all the coins.

Table 3. Physical parameters of the twelve coins.

Coin	Weight g	Density	
		Experimental	Calculated
Aes Litra (#1)	3.51	8.33	7.79
Rostrum tridens (#2)	28.78	8.94	8.67
Mercurius/Prora (#3)	4.34	7.75	8.02
Augustus (#4)	9.19	8.67	8.96
Claudius (#5)	9.33	8.26	9.11
Caligula (#6)	2.54	8.48	8.97
Severus Alexander (#7)	10.69	8.91	9.01
Philippus II Caesar (#8)	18.41	8.41	8.09
Divus Claudius II Gothicus (#9)	1.61	7.66	9.20
Galerius Maximian (#10)	2.59	8.37	8.98
Valens (#11)	2.38	8.52	9.38
Anastasius I (#12)	15.91	7.96	8.94

6. Discussion

6.1. SEM and EMPA

Scanning electron microscopy (SEM) and X-ray maps of the coins provided evidence of (1) the heterogeneous distribution of the Sn, Cu, Pb, and Fe main alloying elements and (2) the corrosion of the surface.

EMPA data permitted the grouping of the coins based on their chemical composition (Table 2). Group 1 consists mainly of Cu (up to 99 wt.%). Conversely, the other groups have a more complex chemical composition, resulting in a greater heterogeneity of the alloys (Table 2, Figure 5).

EMPA data of all the coins plotted in binary diagrams (Figure 5) highlighted the chemical variations in the major elements (Cu, Sn, Pb, Fe). Figure 5a (coin #1, group 2)

shows the chemical variations in Cu and Sn. An important feature of this coin is the content of Sn (up to 94 wt.%, Table 2) due to important processes of Sn enrichment due to corrosion and contextual decuprification in these areas. Figure 5h (group 3) shows the same trend of coin #8 as observed in the previous coin (i.e., high content of Sn), but, in addition, Pb and Fe occur. This composition is very unusual and can be explained in two ways: (1) the corrosion layer is enriched in Sn and depleted in Cu, a typical feature of Cu-Sn-Pb-Zn, Cu-Sn-Pb, and Cu-Sn bronzes [40,41] and (2) during economic crises, the Romans used a tinning covering instead of the more common silvering of the coins for the creation of a surface with a silver-like lustrous appearance [42]. Figure 5b,c,i,g (group 3) illustrate the complex chemical variations in the alloy and reveal the highest Pb contents. In particular, coin #3 (Figure 5c) shows an unusual enrichment in Pb in micro-areas (up to 99 wt.%). Figure 5e,l (group 4) illustrate the pattern of the Cu-Pb coins, an alloy utilized by Romans, as Pb improves the chemical and physical features.

The *subaerata* coin #11 shows two distinct compositions: Cu on the surface and Pb in the inner areas (Figure 5k). The significant enrichment in Fe shown by some coins is related to the use of the sulfide ore (chalcopyrite) as the Cu source.

Concerning trace elements, Au, Ag, Zn, As, Sb, Cd, Co, and Ni are relevant in attempting to identify the sources of the base metal ores. All coins are devoid of Au, except Aes of Claudius (#5), which shows in some micro-areas Au enrichment, of up to 1.48 wt.%. The silver content is low in the copper and copper–tin groups and enriched in the copper–tin–lead group, suggesting that silver-rich galena was present in the raw material. Arsenic is present in all coins but is more enriched in the coin (#9), probably due to the presence of arsenian pyrite or arsenopyrite in the raw materials. Zinc and antimony also occur as trace elements in some coins (Table 2). Minor amounts of Cd, Co, and Ni also occur. The occurrence of all these trace elements suggests that the starting material used for the production of the alloy was made of different sulfides, probably coming from various deposits.

It is reasonable to assume, based on the chemical composition (major, minor, and trace elements) of the coins, that over all these centuries the quality of bronze can be correlated with the availability of ore sources, the economic crises affecting the life of Romans, and the predominant use of lead for its chemical and physical properties.

The results showed that the degree of chemical heterogeneity versus the age of minting increased from the Republican Age to the Imperial Age. Indeed, the Republican coins are mainly made of Cu and Cu-Sn alloy, whereas the Imperial coins are a ternary Cu-Sn-Pb alloy. This observation could be ascribed to the Romans' knowledge of the chemical and physical properties of metals which favored the production of more complex alloys in the Imperial time.

6.2. XRD and FTIR

X-ray diffraction patterns of the patinas on coins revealed the presence of some crystalline compounds such as a copper–tin alloy, cuprite (Cu_2O), stannic oxide (SnO_2), $CuAl_2O_4$, and carbonate of Pb and Cu (Figure 6). Indeed, a layer of cuprite grows on a copper alloy artifact as a result of the metal–oxygen interaction due to an electrochemical process. This layer can be considered a membrane able to conduct ions through it. As the bronze coins also contain tin in the alloy, its reaction with oxygen led to the formation of stannic oxide SnO_2 (or cassiterite), which can form, by hydration, stannic acid. Consequently, the early-formed cuprite, being more soluble than stannic oxide, has the tendency to be leached and to migrate to the environment, involving an anomalous increase in Sn on the surface. Indeed, in the corrosion layer, enrichment and depletion of Sn and Cu, respectively, are typical features of bronzes [41,42]. This phenomenon, along with the possible tinning of some coins, can explain the Sn-enriched layer (e.g., coins #1 and 8#), which forms through the internal oxidation of Sn accompanied by the selective dissolution of Cu [43].

Commonly, the occurrence of traces of $CuAl_2O_4$ spinel can be explained by the use of nano $CuAl_2O_4$ spinel to minimize copper leaching. This is an environmentally friendly strategy for antibacterial application. In our case, the occurrence of this synthetic phase

is probably due to the application of synthetic $CuAl_2O_4$ on coins by private collectors to stabilize their collections [44,45].

Figure 7 reports the FTIR spectra of green compounds: a mixture of malachite, hydrocerussite, acidic carbonate, and probably double carbonate and hydrated carbonate. The range 4000–600 cm^{-1} shows the vibrational modes of H_2O, OH, and CO_3^{2-}, which are in agreement with those reported in the literature [39]. Figure 4 illustrates the internal modes of carbonates of coins #8 and #12 in which those of CO_3^{2-} appear as sharp bands in coin #12 (1122, 1070, 896, 764 cm^{-1}) and lesser defined bands in coin #8. These complex patterns of bands indicate that cerussite and hydrocerussite occur in association with malachite [39]. The stretching of the hydroxyl group and the H_2O molecule gives rise to broad bands in the region near 3500–3400 cm^{-1} (Figure 7). The compounds in the copper sources patina of the bronzes suggest a complex interaction between metal, H_2O, and CO_2 involving the formation of a composite mineral assemblage such as oxides, hydroxides, and carbonates of Cu and Pb.

6.3. Density

The experimental density generally is lower than the calculated density because the coins are damaged by corrosion and alteration. Generally, dual-phase or multi-phase alloys have been revealed to be likely to attack micro-galvanic corrosion, thus giving an inhomogeneous distribution of the metals [43]. Differences between the inner part and de-alloyed surfaces can also contribute to these differences. Only coins #5 and #9 show some difference between the two densities, probably linked to the presence of different Pb-bearing phases or concentrations.

In Figure 8, the two trends show very good agreement as a mark of the quality of the average composition illustrated by EMP analyses.

7. Conclusions

A multi-analytical approach has been used to study a set of Roman bronze coins. We performed numismatic identification, chemical composition, and identification of corrosion products. The following specific conclusions can be drawn:

1. The coins show a heterogeneous distribution of the main components of the alloy (e.g., Sn, Cu, Pb, Fe), excluding the *subaerata* coin.
2. EMP analyses permit us to group the coins into five groups: (1) copper, (2) copper–tin alloy, (3) copper-leaded alloy, (4) copper–tin lead alloy, and (5) one *subaerata* coin.
3. The degree of chemical heterogeneity versus the age of minting increases from the Republican Age to the Imperial Age
4. The surface heterogeneity of the coins is a consequence of selective corrosion processes affecting metals such as copper and tin and pseudomorphic replacement of the alloy by the corrosion products. This phenomenon may occur due to common events in the long-term corrosion of archaeological bronzes in soil, identified as decuprification and destannification.
5. Concerning patinas, FTIR data indicated that the products of the patina are mainly oxides, hydroxides, and carbonates. These data along with chemical and structural characterization can be instrumental in artifact conservation, particularly in the selection of inhibitors. Furthermore, the periodic monitoring of the chemical composition of the coin surfaces permits assessments of the evolution of corrosive processes and, if necessary, adjustments to conservation strategies.
6. The variability of major, minor, and trace elements provided important information about the sources of the base metal ores used to produce coins widely distributed in Rome and its provinces. It also suggests the deliberate addition of lead during the Imperial Age.

Author Contributions: C.D.V., C.A. and M.B.: conceptualization, formal analysis, data interpretation, funding acquisition, and original draft preparation. F.C.: numismatic analysis. A.M.C., S.M., T.d.C. and L.M.: review and editing. All authors have read and agreed to the published version of the manuscript.

References

1. Balbi De Caro, S. *La Moneta a Roma e in Italia*, 2nd ed.; Banca d'Italia, Ed.: Milano, Italy, 1993.
2. Kraft, G.; Flege, S.; Reiff, S.; Ortner, H.M.; Ensinger, W. EPMA Investigation of Roman coin silvering techniques. *Microchim. Acta* **2006**, *155*, 179–182. [CrossRef]
3. Dungworth, D. Roman copper alloys: Analysis of artefacts from northern Britain. *J. Archaeol. Sci.* **1997**, *24*, 901–910. [CrossRef]
4. Bodet, A. Greek and Roman Copper Alloy Coins (Fifth Century BC—Third Century AD): From Microstructures to Manufacturing Process. In *Metallography, Microstructure, and Analysis*; Springer: Berlin/Heidelberg, Germany, 2023.
5. Vlachou-Mogire, C. Investigation of the Manufacturing Technology of Complex Copper Alloy Late Roman Coins (240 AD to 395 AD) Using Archaeometallurgy Technique. *Metallogr. Microstruct. Anal.* **2023**, *12*, 202–218. [CrossRef]
6. Julius Caesar, C. *Caesar the Gallic War*; Edwards, H.J., Ed.; Harvard University Press: Cambridge, UK, 1986; Volume 12, pp. 250–251.
7. Hammersen, L.A. The Control of Tin in Southwestern Britain from the First Century A.D. to the Late Third Century A.D. Ph.D. Dissertation, North Caroline State University, Raleigh, NC, USA, 2007.
8. Crawford, M.H. *Roman Republican Coinage*; Cambridge University Press: Cambridge, UK, 1974; Volume I and II.
9. Crawford, M.H. *Coinage and Money under the Roman Republic: Italy and the Mediterranean Economy*; Grierson, P., Ed.; University of California Press: Berkeley, CA, USA, 1985.
10. Panvini Rosati, F. La moneta romana. In *Archeo Numismatica*; L'Erma di Bretschneider: Rome, Italy, 1988; Volume 42.
11. Panvini Rosati, F. *La Moneta Greca e Romana*; L'Erma di Bretschneider: Rome, Italy, 2000; p. 164.
12. Bowman, A.K. *Quantifying the Roman Economy: Methods and Problems*; Bowman, A., Wilson, A., Eds.; Oxford University Press: Oxford, UK, 2009.
13. Harris, W.V. The nature of Roman money. In *The Monetary Systems of the Greeks and Romans*; Harris, W.V., Ed.; Oxford University Press: Oxford, UK, 2008; pp. 174–207.
14. Hollander, D.B. The demand for money in late Roman Republic. In *The Monetary Systems of the Greeks and Romans*; Harris, W.V., Ed.; Oxford University Press: Oxford, UK, 2008; pp. 112–136.
15. Bernareggi, E. *Istituzioni di Numismatica Antica*; Cisalpino-Goliardica, Ed.: Milan, Italy, 1985.
16. Wilson, A.; Friedman, H. Mining Database. Version 1.0. 2010. Available online: http://oxrep.classics.ox.ac.uk/databases/mines_database/ (accessed on 26 November 2023).
17. Baron, S.; Tămaş, C.G.; Cauet, B.; Munoz, M. Lead isotope analyses of gold–silver ores from Roşia Montană (Romania): A first step of a metal provenance study of Roman mining activity in Alburnus Maior (Roman Dacia). *J. Archaeol. Sci.* **2011**, *38*, 1090–1100. [CrossRef]
18. Stos-Gale, Z.A.; Gale, N.H.; Houghton, J.; Speakman, R. Lead isotope analyses of ores from the Western Mediterranean. *Archaeometry* **1995**, *37*, 407–415. [CrossRef]
19. Stos-Gale, Z.A.; Gale, N.H.; Annetts, N. Lead isotope analyses of ores from the Aegean. *Archaeometry* **1996**, *38*, 381–390.
20. Stos-Gale, Z.A.; Maliotis, G.; Gale, N.H.; Annetts, N. Lead isotope characteristics of the Cyprus copper ore deposits applied to provenance studies of copper oxhide ingots. *Archaeometry* **1997**, *39*, 83–124. [CrossRef]
21. Stos-Gale, Z.S.; Gale, N.H. Metal provenancing using isotopes and the Oxford archaeological lead isotope database (OXALID). *Archaeol. Anthropol. Sci.* **2010**, *1*, 195–213. [CrossRef]
22. Klein, S.; von Kaenel, H.M. Metal analysis and numismatic studies of early Roman Imperial Bronze coinage. Part 1: Chemical characterization of copper coins from Augustus to Claudius. *Rev. Suisse Numis.* **2000**, *79*, 53–106.
23. Klein, S.; Rico, C.; Lahaye, Y.; von Kaenel, H.M.; Domergue, C.; Brey, G.P. Copper ingots from the western Mediterranean Sea: Chemical characterization and provenance studies through lead- and copper isotope analyses. *J. Rom. Archaeol.* **2007**, *20*, 203–221. [CrossRef]
24. Klein, S.; Lahaye, Y.; Brey, G.P.; Von Kaenel, H.-M. The early Roman imperial AES coinage II: Tracing the copper sources by analysis of lead and copper isotopes—Copper coins of Augustus and Tiberius. *Archaeometry* **2004**, *46*, 469–480. [CrossRef]
25. Bendall, C.; Wigg-Wolf, D.; Lahaye, Y.; von Kaenel, H.-M.; Brey, G.P. Detecting changes of celtic gold sources through the application of trace element and pb isotope laser ablation analysis of celtic gold coins. *Archaeometry* **2009**, *51*, 598–625. [CrossRef]
26. Bernabale, M.; Cognigni, F.; Mancini, C.; Proietti, A.; Mura, F.; Montanari, D.; Nigro, L.; Rossi, M.; De Vito, C. 3D fractures analysis and conservation assessment of wrought iron javelin through advanced non-invasive techniques. *Sci. Rep.* **2023**, *13*, 10142. [CrossRef]

27. Bernabale, M.; Cognigni, F.; Mura, F.; Nigro, L.; Montanari, D.; Rossi, M.; De Vito, C. 3D imaging of micro-segregation and corrosion behavior of alloying elements in archaeological artefacts from Motya (Sicily, Italy). *Corros. Sci.* **2023**, *211*, 110900. [CrossRef]

28. Di Turo, F.; Coletti, F.; De Vito, C. Investigations on alloy-burial environment interaction of archaeological bronze coins. *Microchem. J.* **2020**, *157*, 104882. [CrossRef]

29. Fabrizi, L.; Di Turo, F.; Medeghini LDi Fazio, M.; Catalli, F.; De Vito, C. The application of non-destructive techniques for the study of corrosion patinas of ten Roman silver coins: The case of the medieval Grosso Romanino. *Microchem. J.* **2019**, *145*, 419–427. [CrossRef]

30. Pais, M.; Rao, P. Biomolecules for corrosion mitigation of zinc: A short review. *J. Bio-Tribo-Corros.* **2019**, *5*, 92. [CrossRef]

31. Argyropoulos, V.; Boyatzis, S.C.; Giannoulaki, M.; Guilminot, E.; Zacharopoulou, A. Organic green corrosion inhibitors derived from natural and/or biological sources for conservation of metals cultural heritage. In *Microorganisms in the Deterioration and Preservation of Cultural Heritage*; Springer: Berlin/Heidelberg, Germany, 2021; 341p. [CrossRef]

32. Abdel-Karim, A.M.; El-Shamy, A.M. A review on green corrosion inhibitors for protection of archeological metal artifacts. *J. Bio-Tribo-Corros.* **2022**, *8*, 35. [CrossRef]

33. Bernabale, M.; Nigro, L.; Montanari, D.; De Vito, C. Exploring the chemical composition and corrosion patterns of arrowheads used in the Siege of Motya (397 BC) through a multi-analytical approach. *J. Cul. Herit.* **2021**, *52*, 146–152. [CrossRef]

34. Dion, R. Le problème des Cassiterides. *Latomus* **1952**, *11*, 306–314.

35. Durali-Mueller, S.; Brey, G.P.; Wigg-Wolf, D.; Lahaye, Y. Roman lead mining in Germany: Its origin and development through time deduced from lead isotope provenance studies. *J. Archaeol. Sci.* **2007**, *34*, 1555–1567. [CrossRef]

36. Muhly, J.D. Sources of tin and the beginnings of bronze metallurgy. *Am. J. Archaeol.* **1985**, *89*, 275–291. [CrossRef]

37. Ferrini, V.; Martarelli, L.; De Vito, C.; Çina, A.; Deda, T. The Koman dawsonite and realgar–orpiment deposit, Northern Albania: Inferences on processes of formation. *Can. Mineral.* **2003**, *4*, 413–427. [CrossRef]

38. Craddock, P.T. The composition of the copper alloys used by the Greek, Etruscan and Roman civilizations. *J. Archaeol. Sci.* **1977**, *4*, 102–123. [CrossRef]

39. White, W.B. The carbonate minerals. In *The Infrared Spectra of Minerals*; Farmer, V.C., Ed.; Mineralogical Society: London, UK, 1974.

40. Constantinides, I.; Adriaens, A.; Adams, F. Surface characterization of artificial corrosion layers on copper alloy reference materials. *Appl. Surf. Sci.* **2002**, *189*, 90–101. [CrossRef]

41. Giumlia-Mair, A. On surface analysis and archaeometallurgy. *Nucl. Instrum. Methods B* **2005**, *239*, 35–43. [CrossRef]

42. Šmit, Ž.; Istenič, J.; Knific, T. Plating of archaeological metallic objects: Studies by differential PIXE. *Nucl. Instrum Methods B* **2008**, *266*, 2329–2333. [CrossRef]

43. Robbiola, L.; Blengino, J.M.; Fiaud, C. Morphology and mechanisms of formation of natural patinas on archaeological Cu–Sn alloys. *Corros. Sci.* **1998**, *40*, 2083–2111. [CrossRef]

44. Wang, Z.; Liang, K.; Chan, S.W.; Tang, Y. Fabrication of nano $CuAl_2O_4$ spinel for copper stabilization and antibacterial application. *J. Hazard. Mater.* **2019**, *371*, 550–557. [CrossRef] [PubMed]

45. Lv, W.; Liu, B.; Qiu, Q.; Wang, F.; Luo, Z.; Zhang, P.; Wei, S. Synthesis, characterization and photocatalytic properties of spinel CuAl2O4 nanoparticles by a sonochemical method. *J. Alloys Compd.* **2009**, *479*, 480–483. [CrossRef]